JPE 13-2-4

http://dx.doi.org/10.6113/JPE.2013.13.2.206

Investigation and Implementation of a Passive Snubber with a Coupled-Inductor in a Single-Stage Full-Bridge Boost PFC Converter

Tao Meng[†], Hongqi Ben[*], Chunyan Li[**], and Guo Wei[*]

[†*]School of Electrical Engineering and Automation, Harbin Institute of Technology, Harbin, China
[**]School of Mechanical and Electrical Engineering, Heilongjiang University, Harbin, China

Abstract

In this paper, an improved passive snubber is investigated in a single-phase single-stage full-bridge boost power factor correction (PFC) converter, by which the voltage spike across primary side of the power transformer can be suppressed and the absorbed energy can be transferred to the output side. When compared with the basic passive snubber, the two single-inductors are replaced by a coupled-inductor in the improved snubber. As a result, synchronous resonances in the snubber can be achieved, which can avoid the unbalance of the voltage and current in the snubber. The operational principle of the improved passive snubber is analyzed in detail based on a single-phase PFC converter, and the design considerations of both the snubber and the coupled-inductor are given. Finally, a laboratory-made prototype is built, and the experimental results verify the feasibility of the proposed method and the validity of the theoretical analysis and design method.

Key words: Coupled-inductor, Full-bridge, Passive snubber, Power factor correction (PFC), Single-stage

I. INTRODUCTION

In the research field of power factor correction (PFC), single-stage PFC integrates the functions of PFC and isolated DC/DC conversion into a single power converter, and it has advantages such as high efficiency, simplicity and low cost when compared with two-stage PFC [1], [2]. In recent years, many low power single-stage PFC converters have been investigated. However, fewer high power schemes have been proposed [3].

The isolated full-bridge boost topology is attractive in applications of medium and high power single-stage PFC. The reasons why this type of PFC has not been widely used can be attributed to: 1) an additional starting-up circuit is required to establish an initial output voltage, and 2) there is a voltage spike across the bridge leg caused by the transformer leakage inductor [4], [5]. For normal single-stage full-bridge boost PFC, starting-up has been realized through many efficient methods. For example, flyback starting schemes are proposed in [4]-[6], and a direct starting mode of the converter in the state of no load is presented in [7].

To suppress the voltage spike, a number of techniques have been proposed. Methods based on the basic active clamping technique are introduced in [8]-[10], and they has been the most widely investigated [11]. Two new active clamping techniques were proposed in [12], [13]. A two-switch clamping circuit was presented in [14]. Some active auxiliary circuits with a single-switch are adopted in [11], [15] and [16]. The voltage spike is efficiently suppressed after the adoption of each of the above active methods. However, the active methods above have a common drawbacks, that is: one (or two) additional switch is introduced, which increases the complexity of the control circuit and reduces the reliability of the whole system. Moreover, the switching frequency of the additional switch is two times as high as that of the main switches, so it is difficult to choose the switch. Besides the active methods, some passive methods have also been proposed. For example, LC resonance schemes have been studied in [17]-[19], which

Manuscript received Sep. 19, 2012; revised Jan. 5, 2013
Recommended for publication by Associate Editor Joung-Hu Park.
[†]Corresponding Author: mengtao@hit.edu.cn
Tel: +86-451-86413602, Fax: +86-451-86413602, Harbin Institute of Technology
[*]School of Electrical Engineering and Automation, Harbin Institute of Technolgy, China
[**]School of Mechanical and Electrical Engineering, Heilongjiang University, China

can also achieve soft switching of the main switches. However, its resonance energy can not be transferred to the load. Instead, it is added to the conduction losses of the converter. A RCD snubber is used in [20], but the energy of the snubber circuit is released by the resister. A passive clamping technique is proposed in [21]. However, the problem of the magnetic bias of the power transformer appears after the adoption of the passive clamping circuit. A passive snubber is investigated in [22]. However, after the adoption the passive snubber, a diode is connected in series with the bridge leg switches, which will reduce the efficiency of the converter. In [23], another passive snubber is investigated in three-phase single-stage PFC which overcomes the disadvantage of the snubber in [22]. However, an unbalance of the voltage and current appears between the two resonant circuits.

In this paper, based on the passive snubber in [23], an improved passive snubber is investigated in a single-phase single-stage full-bridge boost PFC converter. In the improved snubber, the two single-inductors are replaced by a coupled-inductor. Theoretical analysis and experimental results show that the voltage spike can be suppressed efficiently after adoption of the improved snubber. It can also overcome the drawback of the passive snubber in [23].

II. THE PFC CONVERTER AND ITS PRINCIPLE

A. The PFC Converter

A single-phase single-stage full-bridge boost PFC converter is shown in Fig.1, where the improved passive snubber is composed of C_1, C_2 (C_1=C_2), D_{C1}, D_{C2}, D_C and the coupled-inductor (L_1=L_2 are equivalent inductances). D_{S1}~D_{S4} and C_{S1}~C_{S4} are the parasitic components of switches S_1~S_4. L_{lk} and n are the equivalent leakage inductance and the voltage ratio of transformer T, respectively. The switching mode of S_1~S_4 is the same as that in [23]. The converter in Fig.1 operates in the continuous current mode (CCM). When the bridge leg switches are shorted (S_1 & S_2 or S_3 & S_4 are turning on), the boost inductor L is charged by u_i, and the input current increases almost linearly. When the bridge diagonal-leg switches turn on (S_2 & S_3 or S_1 & S_4 are turning on), the output current is provided by u_i and L, and the input current decreases. The process above is repeated periodically, the input current follows the input voltage, and both PFC and AC/DC conversion can be achieved.

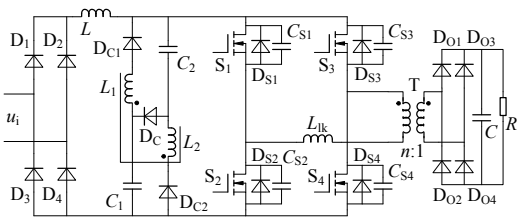

Fig. 1. PFC converter with improved passive snubber.

B. Analysis of the Operational Process

The working process of the snubber is closely related to the principle of the PFC converter, and the special control strategy has not been introduced for the snubber. The PFC converter in Fig.1 operates in CCM, which is different than the converter in [23]. As a result, its operational process is presented as followed for further analysis and design.

To simplify the analysis, it is assumed that: 1) all of the devices are ideal, 2) the capacitor C is large enough, so that the output voltage U_o can be considered as a constant value, and 3) during one charging period of L, the change of u_i is negligible because the charging period is much shorter than the line period. The following analysis is during one charging period of L when u_i>0. The theoretical waveforms and the equivalent circuits of the different stages are shown in Fig.2 and Fig.3, respectively.

Stage 1 (before t_0): S_2 and S_3 are turning on, while S_1 and S_4 are turning off. The voltage across the primary side of transformer T is U_k=nU_o, and U_{C1}=U_{C2}=nU_o/2, U_{CS1}=U_{CS4}=nU_o, and U_{CS2}=U_{CS3}=0. The current in L (i_L) flows through S_2, S_3 and T to the load, and it decreases. On the secondary side of T, D_{O1} and D_{O4} are turning on, and D_{O2} and D_{O3} are turning off.

Stage 2 (t_0-t_1): At t_0, S_1 turns on, and S_3 turns off. L is charged by u_i, and i_L increases linearly. In the snubber, C_1 is resonant with L_1 through D_{C1}, S_1 and S_2. Furthermore, C_2 is resonant with L_2 through S_1, S_2 and D_{C2}. The current of L_{lk} (i_{Llk}) can not be mutated, so i_{Llk} flows through S_2, D_{S4} and T to the load and i_{Llk} decreases immediately. At t_1, i_{Llk} reduces to zero (the excitation current of T is not considered here), and D_{O1} and D_{O4} are turned off. The inductance of L_{lk} is very small, so the duration of this stage can be ignored.

Stage 3 (t_1-t_2): The resonances in stage 2 are continuous. The voltage of C_1 and C_2 and the current in L_1 and L_2 are:

$$u_{C1/C2}(t)=\frac{nU_o}{2}\cos\frac{1}{\sqrt{L_1C_1}}(t-t_1) \tag{1}$$

$$i_{L1/L2}(t)=\frac{nU_o}{2}\sqrt{\frac{C_1}{L_1}}\sin\frac{1}{\sqrt{L_1C_1}}(t-t_1) \tag{2}$$

At t_2, U_{C1}=U_{C2}=0, and the energy of C_1 and C_2 is transferred to L_1 and L_2 entirely. The duration of this stage is calculated as:

$$t_{12}=\frac{\pi}{2}\sqrt{L_1C_1} \tag{3}$$

Stage 4 (t_2-t_3): In this stage, i_L still increases linearly and the output current is provided by capacitor C alone. The voltage of C_1 or C_2 is zero, so that diode D_C is turned on, L_1 is connected in series with L_2, and their current flows through D_{C1}, S_1, S_2, D_{C2} and D_C. During stage 1~4, U_{CS3} is still zero, so that S_3 turns off with zero voltage at t_0.

Stage 5 (t_3-t_4): At t_3, S_2 turns off, and S_4 turns on with zero voltage. C_{S2}, C_{S3}, C_1 and C_2 are charged by L_1, L_2 and L. The voltage across the bridge leg increases from zero, so that S_2

turns off with zero voltage. The capacitance of C_{S1}~C_{S4} is much small than that of C_1 and C_2. Therefore, only the charging process of C_1 and C_2 is considered in the following calculation. In this stage, the following relationships can be obtained:

$$C_1 \frac{\mathrm{d}u_{C1/C2}(t)}{\mathrm{d}t} = i_L(t_3) + i_{L1/L2}(t) \tag{4}$$

$$u_{C1/C2}(t) = -L_1 \frac{\mathrm{d}i_{L1/L2}(t)}{\mathrm{d}t} \tag{5}$$

From (4) and (5), the following differential equation is obtained:

$$L_1 C_1 \frac{\mathrm{d}^2 u_{C1/C2}(t)}{\mathrm{d}t^2} + u_{C1/C2}(t) = 0 \tag{6}$$

This equation (6) has the following initial data:

$$u_{C1/C2}(t_3) = 0 \tag{7}$$

$$i_{L1/L2}(t_3) = \frac{nU_o}{2}\sqrt{\frac{C_1}{L_1}} \tag{8}$$

Therefore, the voltage expression of C_1 or C_2 and the current expression of L_1 or L_2 can be obtained:

$$u_{C1/C2}(t) = [\sqrt{\frac{L_1}{C_1}} i_L(t_3) + \frac{nU_o}{2}]\sin\frac{t}{\sqrt{L_1 C_1}} \tag{9}$$

$$i_{L1/L2}(t) = i_L(t_3)(\cos\frac{t}{\sqrt{L_1 C_1}} - 1) + \frac{nU_o}{2}\sqrt{\frac{C_1}{L_1}}\cos\frac{t}{\sqrt{L_1 C_1}} \tag{10}$$

At t_4, the charging process of C_1 and C_2 is over. Therefore, U_k= -nU_o, U_{C1}=U_{C2}=nU_o/2, U_{CS1}=U_{CS4}=0, and U_{CS2}=U_{CS3}=nU_o. In this stage, the output current is only provided by capacitor C. The inductance of L is large enough, so that the change of i_L can be ignored during this stage. During the whole line period, the value of $i_L(t_3)$ is varying, so that the duration of this stage is different during the whole line period.

Stage 6 (t_4-t_5): In this stage, the current of L_1, L_2 and L flows through S_1, S_4 and T to the load, and then it decreases. On the secondary side of T, D_{O2} and D_{O3} turn on. In this stage, the expression of $i_{L1}$and i_{L2} is:

$$i_{L1/L2}(t) = i_{L1/L2}(t_4) - \frac{nU_o}{2L_1}(t - t_4) \tag{11}$$

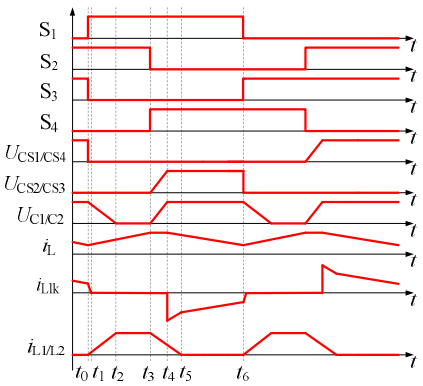

Fig. 2. Theoretical waveforms.

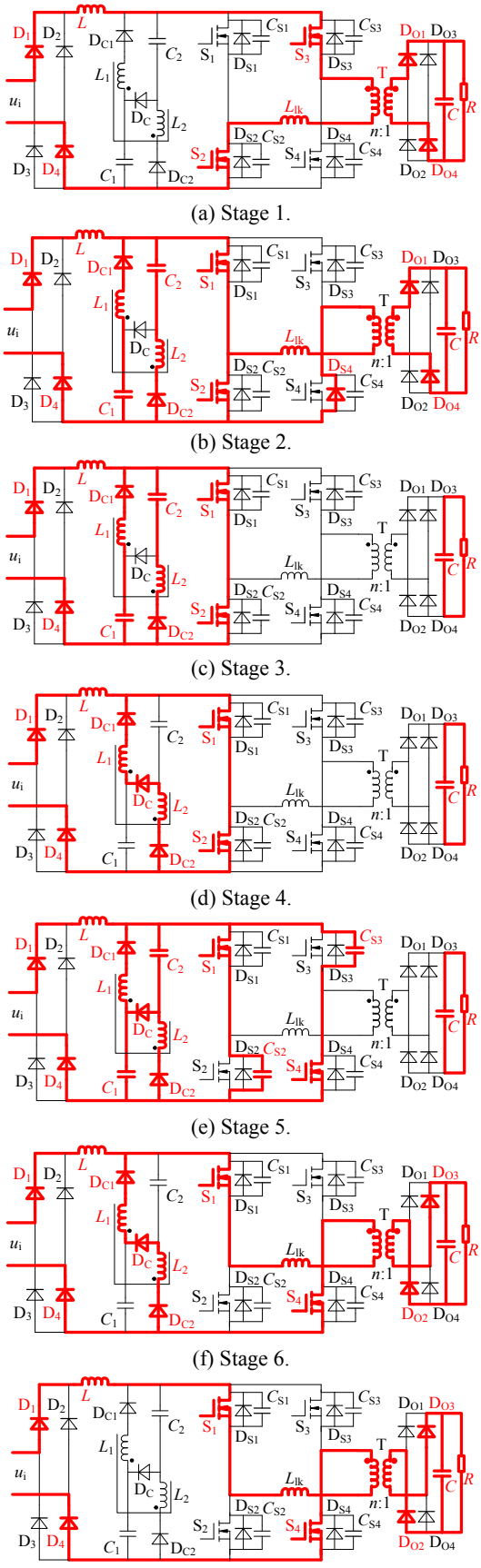

Fig. 3. Equivalent circuit of each stage.

At t_5, i_{L1} and i_{L2} reduce to zero. The inductance of L_{lk} is so small that the rising process of i_{Llk} is ignored in this stage.

Stage 7 (t_5-t_6): In this stage, i_L flows through S_1, S_4 and T to the load, and it still decreases, which is similar to that in stage 1.

After t_6, the converter operates in another charging period, and the switching state between S_1 and S_3, and S_2 and S_4 are exchanged.

C. Analysis of Parameters in the snubber

According to the analysis in [23] and the analysis above, the voltage and current stress of switches S_1~S_4 in Fig.1 can be calculated:

$$U_S = nU_o + i_L(t)\sqrt{\frac{2L_{lk}}{C_1}}\sin\frac{\sqrt{2}t}{\sqrt{L_{lk}C_1}} \tag{12}$$

$$I_S = I_{Lmax} + 2i_{L1/L2}(t_2) = I_{Lmax} + nU_o\sqrt{\frac{C_1}{L_1}} \tag{13}$$

The duration of stage 2 is so small that i_{Llk} is ignored in the calculation of the current stress of S_2 or S_4. It can be seen that U_S decreases as C_1 increases, and that I_S increases as C_1 increases or L_1 decreases.

According to the analysis in [23], the first limitation of L_1 and C_1 can be obtained:

$$L_1C_1 \le 2.87D_{min}{}^2T^2 \tag{14}$$

Where D=(t_3-t_0)/T is the duty cycle of the PFC converter, and T is the charging period of L.

In [23], the three-phase PFC converter operates in discontinuous current mode (DCM). Generally, its duty cycle is within 50%, so the current in L_1 or L_2 must reduce to zero during the phase when the bridge diagonal-leg switches are turning on. However, in this paper, the single-phase PFC converter operates in CCM. Therefore, the maximum duty cycle will be much more than 50%, so another constraint condition of L_1 and C_1 must be analyzed to make sure that the current in L_1 and L_2 can reduce to zero in order to avoid the magnetic saturation of L_1 and L_2 after several charging period.

The current in L_1 and L_2 begins to decrease during stage 5, and it can be see from (10) that $i_{L1/L2}(t)$ will decrease faster as $i_L(t_3)$ increases. It also needs to be made certain that $i_{L1/L2}(t)$ can reduce to zero when $i_L(t_3)$=0. In that case, the energy of L_1 and L_2 will be transferred to C_1 and C_2 entirely. Therefore, the following relationship can be obtained:

$$\frac{\pi}{2}\sqrt{L_1C_1} \le (1-D_{max})T \tag{15}$$

From (15), the second limitation of L_1 and C_1 can be obtained:

$$L_1C_1 \le \frac{4(1-D_{max})^2T^2}{\pi^2} \tag{16}$$

From the analysis above, it can be seen that the voltage stress of D_{C1} or D_{C2} is equal to that of C_1 or C_2, which is U_S/2. It can also be seen that the voltage stress of D_C is U_S, the current stress of D_{C1} or D_{C2} is equal to that of L_1 or L_2, which can be obtained from (8), and the current stress of D_C is equal to that of S_1~S_4, which can obtained in (13).

III. Design Considerations of the Coupled-Inductor

A. Mechanism Analysis of the Coupled-Inductor

In section II, it was proposed that C_1=C_2 and L_1=L_2. Therefore, the resonances between C_1 (or C_2) and L_1 (or L_2) are synchronous. However, there are some differences between two capacitors with the same capacitance. This is due to their tolerance features. For the same reason, the inductances of two inductors with the same configuration are not exactly the same. Therefore, the resonances between C_1 (or C_2) and L_1 (or L_2) are asynchronous, which would result in an unbalance of the voltage and current between C_1 and C_2, L_1 and L_2, and D_{C1} and D_{C2}. In actual fact, to avoid over voltage on the capacitors (C_1 or C_2) and the diodes (D_{C1}, D_{C2} or D_C) and to avoid saturation of the inductors (L_1 or L_2), capacitors and diodes with a higher voltage or current stress and inductors with a larger magnetic core volume must be considered.

To resolve this problem, the coupled-inductor is adopted. Here, the two inductors (L_1 and L_2) are made on a common magnetic core, and they have a common magnetic circuit and the same number of turns. Therefore, the difference in the inductances of the two inductors can be ignored. As a result, the asynchronous resonances brought from the difference between the two inductors have not been considered.

The resonances between C_1 (or C_2) and L_1 (or L_2) appear in stage 2, 3 and 5. The following analysis is based on the circuit models in Fig.4 and Fig.5, which show the equivalent circuit of the passive snubber in stage 2, 3 and 5. The model of the coupled-inductor is made up of L_{lk1}, L_{m1}, L_{lk2}, L_{m2}, and T_{ideal}, where L_{lk1} and L_{lk2} are the leakage inductance, L_{m1} and L_{m2} are the excitation inductance (L_{lk1}+L_{m1}=L_1, L_{lk2}+L_{m2}=L_2), and T_{ideal} is the ideal transformer. The two inductors have a common magnetic circuit and the same number of turns, so the difference in the inductance between them can be ignored. Therefore: L_{lk1}=L_{lk2} and L_{m1}=L_{m2}. Here, it has been defined that:

$$L_{m1} = aL_1, \quad L_{lk1} = (1-a)L_1 \tag{17}$$

Whrere, 0<a<1.

For Fig.4, it has been defined that the time t_M ($t_0 \le t_M \le t_2$), before t_M, U_{C1}=U_{C2} and i_{L1}=i_{L2}. It is assumed that a difference appears between U_{C1} and U_{C2} after t_M.

$$U_{C2}(t_M) = U_{C1}(t_M) + \Delta U \tag{18}$$

Where ΔU>0.

After t_M, the following relationships are obtained:

$$\begin{cases} i_{L1}(t) = i_{L1}(t_M) + \int_{t_M}^{t} \dfrac{U_{C1}(t) - U_{Ti}(t)}{L_{lk1}} dt \\ i_{L2}(t) = i_{L2}(t_M) + \int_{t_M}^{t} \dfrac{U_{C2}(t) - U_{Ti}(t)}{L_{lk2}} dt \end{cases} \quad (19)$$

$$i_{L1}(t) + i_{L2}(t) = i_{L1}(t_M) + i_{L2}(t_M) + \int_{t_M}^{t} [\frac{U_{Ti}(t)}{L_{m1}} + \frac{U_{Ti}(t)}{L_{m2}}] dt \quad (20)$$

From (19) and (20), the following is obtained:

$$U_{Ti}(t) = \frac{a}{2}[U_{C1}(t) + U_{C2}(t)] \quad (21)$$

From (18), (19), (21), the following expression is obtained:

$$\begin{cases} i_{L1}(t) = i_{L1}(t_M) + \int_{t_M}^{t} \dfrac{(1-a)U_{C1}(t) - \frac{1}{2}a\Delta U}{(1-a)L_1} dt \\ i_{L2}(t) = i_{L2}(t_M) + \int_{t_M}^{t} \dfrac{(1-a)U_{C1}(t) + \Delta U - \frac{1}{2}a\Delta U}{(1-a)L_1} dt \end{cases} \quad (22)$$

From (22), it can be seen that after t_M, $i_{L1}<i_{L2}$, which can help accelerate the discharging of C_2. Furthermore, the following expression can be obtained:

$$\Delta I = i_{L2}(t) - i_{L1}(t) = \int_{t_M}^{t} \frac{(1+a)\Delta U}{(1-a)L_1} dt \quad (23)$$

From (23), it can be seen that ΔI increases as the value of a increases, and that the synchronous changing of between U_{C1} and U_{C2} can be achieved more easily.

After t_M, the expression of $i_{L1}+i_{L2}$ can be obtained from (20) and (21):

$$i_{L1}(t) + i_{L2}(t) = i_{L1}(t_M) + i_{L2}(t_M) + \int_{t_M}^{t} [\frac{U_{C1}(t)}{L_1} + \frac{U_{C2}(t)}{L_2}] dt \quad (24)$$

It can be seen from (24) that $i_{L1}+i_{L2}$ is independent of ΔU. Therefore, the magnetic core excitation of the coupled-inductor can not be affected by the value ΔU.

The same analysis procedure can also be suitable in Fig. 5, which does not have to be repeated.

B. Design of the Coupled-Inductor

According to the analysis above, the configuration scheme of the coupled-inductor is designed as shown in Fig. 6, where the two inductors are made on a common magnetic core, and they have the same number of turns.

From the coupled-inductor theory, the basic mathematical model of the coupled-inductor is:

$$\begin{cases} u_{L1} = L_{11}\dfrac{di_{L1}}{dt} + M\dfrac{di_{L2}}{dt} \\ u_{L2} = L_{22}\dfrac{di_{L2}}{dt} + M\dfrac{di_{L1}}{dt} \end{cases} \quad (25)$$

Where $L_{11}=L_{22}$ are the self inductances and M is the mutual inductance.

The two inductors have a common magnetic circuit, so the following relationship can be obtained approximately:

$$M = L_{11} = L_{22} \quad (26)$$

If the asynchronous resonances in the snubber is ignored, the following can be obtained: $u_{L1}=u_{L2}$ and $i_{L1}=i_{L2}$. Therefore, the following relationship can be obtained approximately:

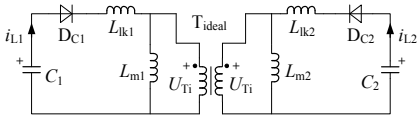

Fig. 4. Equivalent circuit of the snubber in stage 2 and 3.

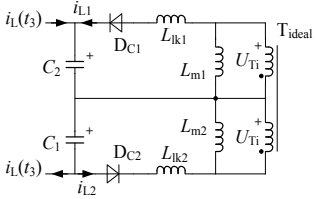

Fig. 5. Equivalent circuit of the snubber in stage 5.

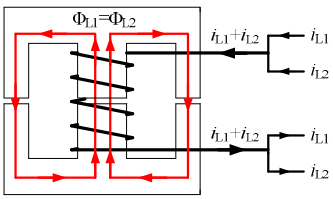

Fig. 6. The configuration scheme of the coupled-inductor.

$$\begin{cases} u_{L1} = L_1\dfrac{di_{L1}}{dt} = 2L_{11}\dfrac{di_{L1}}{dt} \\ u_{L2} = L_2\dfrac{di_{L2}}{dt} = 2L_{22}\dfrac{di_{L2}}{dt} \end{cases} \quad (27)$$

From (27), the relationship between the equivalent inductance and the self inductance of the coupled-inductor can be obtained approximately:

$$L_1 = L_2 = 2L_{11} = 2L_{22} \quad (28)$$

From (27), the following expression can also be calculated:

$$u_{L1} = L_{11}\frac{d(i_{L1} + i_{L2})}{dt} \quad (29)$$

From (29), it can be seen that the coupled-inductor can be equivalent to a single-inductor, of which the inductance is L_{11} and the current is $i_{L1}+i_{L2}$.

Generally, the following expression can be used when the magnetic core of a single-inductor being designed:

$$AP = A_w A_e = \frac{LI_{max}^2}{BJK} \quad (30)$$

Where, A_w and A_e are window area and cross sectional area of the magnetic core, B is the maximum magnetic induction intensity, J is the current density and K is the utilization of the window area.

Therefore, for the coupled-inductor, AP can be calculated:

$$AP_C = \frac{L_{11}I_{Cmax}^2}{BJK} \quad (31)$$

If two single-inductors (L_1 and L_2) are used in the snubber, their AP value can be calculated:

$$\begin{cases} AP_{L1} = \dfrac{L_1 I_{L1max}^2}{BJK} \\ AP_{L2} = \dfrac{L_2 I_{L2max}^2}{BJK} \end{cases} \quad (32)$$

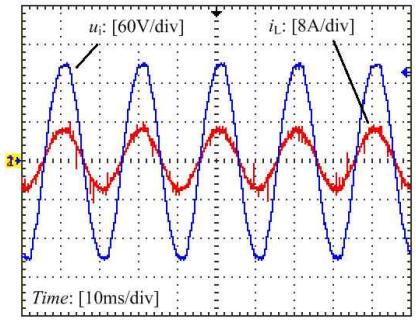

Fig. 7. Input voltage and current.

TABLE I
EXPERIMENTAL DATA

P_o/W	100	200	300	400	500
PF	0.993	0.995	0.997	0.999	0.998
η_C/%	75.5	82.7	87.5	89.4	91.2
η_S/%	75.4	82.3	86.7		

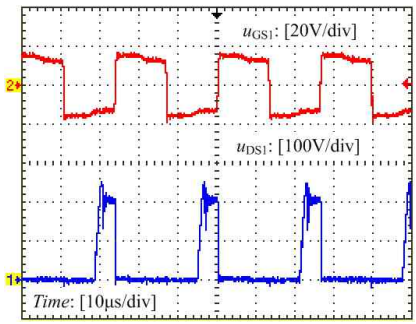

(a) Driving signal and voltage of S_1.

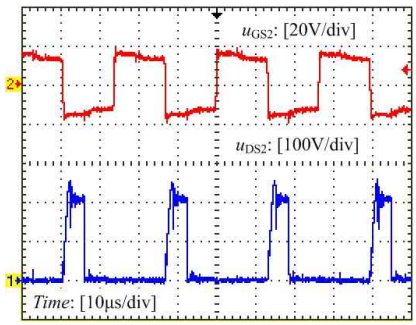

(b) Driving signal and voltage of S_2.

Fig. 8. Soft switching waveforms.

Under ideal conditions, the resonances in a snubber with two single-inductors are synchronous, and the following can be obtained: $I_{L1max}=I_{L2max}=I_{Cmax}/2$. Therefore, expression (33) can be obtained:

$$AP_C = AP_{L1} + AP_{L2} \tag{33}$$

Under real conditions, the resonances in a snubber with two single-inductors are asynchronous, so the maximum currents of L_1 or L_2 increase. However, the maximum current of the coupled-inductor has not been changed. Therefore, under real conditions, the volume of the snubber with a coupled-inductor is smaller than that of the snubber with two single-inductors.

IV. EXPERIMENTAL VERIFICATIONS

To verify the theoretical analysis and the evaluations mentioned above, a laboratory-made prototype of the converter was built, in which the average current mode control strategy was adopted. The basic circuit parameters and the main utilized component types are: u_i=110Vrms±10%, U_o=100Vdc, P_{omax}=500W, L=0.58mH, C=1000μF, L_{lk}=6μH, n=2, and S_1~S_4: 24N60C3 (Infineon, R_{DSmax}=0.16Ω, with a switching frequency of about 37kHz). In the snubber, $C_1=C_2$=44nF±10% (the two capacitors CBB223K are connected in parallel), and $L_{11}=L_{22}$=38μH (EI28, $L_1=L_2$=76μH, the value of L_{lk1} or L_{lk2} is within 2μH, and a>0.97).

Fig. 7 shows the input waveforms of the PFC converter. Table I shows the experimental data for the power factor (PF), the efficiency (η_C) and the efficiency when two single-inductors are adopted (η_S) according to the output power (P_o) variation. When two single-inductors are adopted, asynchronous resonances occur in the snubber. As a result, the experiment is only within 300W to protect the circuit. It can be seen that a good PFC effect has been achieved, and that the prototype shows good performance in conversion efficiency. Fig.8 shows the experimental waveforms of the switches S_1 and S_2. It can be seen that S_1 turns off with zero voltage, and S_2 turns on and off with zero voltage. The switching states of S_3 and S_4 are the same as those of S_1 and S_2. Therefore, the related experimental results are not presented here.

To verify the above analysis, two single-inductors with the same structure have been constructed (EI25, where the inductance $L_1=L_2$=76μH). Fig.9 and 10 are the experimental results (the efficiency data is shown in Table I). To protect the circuit, the results of Fig.9 and 10 are obtained under a relative low bus voltage.

Fig. 9 shows the voltage waveforms of C_1 and C_2, when the two single-inductors are adopted. It can be seen that regardless of whether $C_1=C_2$ or $C_1\neq C_2$, the voltage between C_1 and C_2 is unbalanced, which is the same as saying that the resonances between C_1 (or C_2) and L_1 (or L_2) are asynchronous. Furthermore, the following conclusion can be obtained from Fig.9: the asynchronous resonances in the snubber become more serious as the difference of between C_1 and C_2 increases.

Fig.10 shows the voltage waveforms of C_1 and C_2, when the coupled-inductor is adopted. It can be seen that regardless of whether $C_1=C_2$ or $C_1\neq C_2$, the voltage between C_1 and C_2 is balanced, which is the same as saying that the resonances between C_1 (or C_2) and L_1 (or L_2) are synchronous after the coupled-inductor is adopted. Fig.9 and 10 prove the analysis in section III A. Furthermore, comparing the experimental results in Fig.9 (c) with those in Fig.10 (c), it can be seen that the charging and discharging time of the capacitors are approximately equal when two single-inductors and a coupled-inductor are adopted, respectively. From this, it can

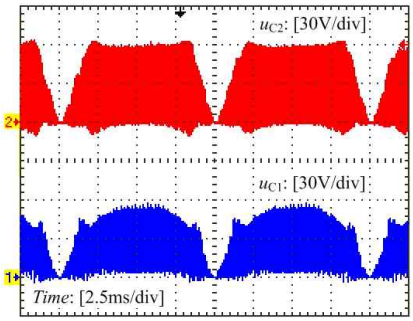

(a) Voltage of C_1 and C_2.

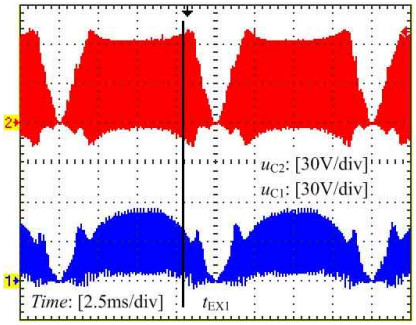

(b) Voltage of C_1 and C_2 when C_1 is connected in parallel with an additional capacitor CBB472J (4.7nF±5%).

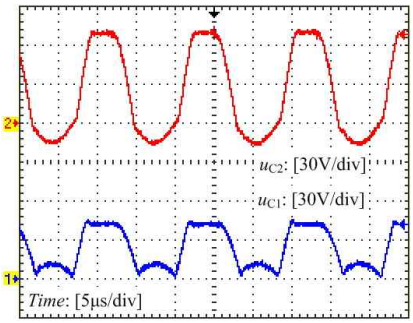

(c) The expanding waveforms of Fig.9 (b) at t_{EX1}.

Fig. 9. Voltage waveforms of with two single-inductors.

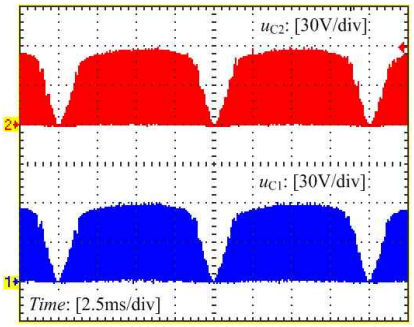

(a) Voltage of C_1 and C_2.

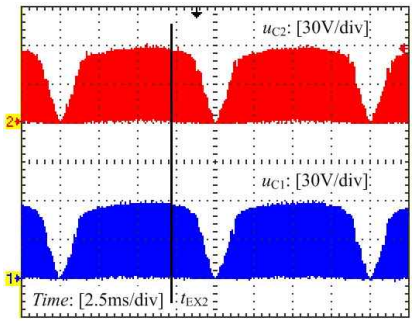

(b) Voltage of C_1 and C_2 when C_1 is connected in parallel with an additional capacitor CBB472J (4.7nF±5%).

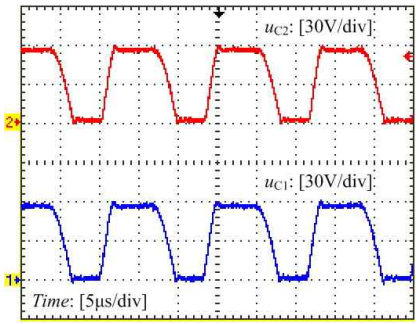

(c) The expanding waveforms of Fig.10 (b) at t_{EX2}.

Fig. 10. Voltage waveforms with a coupled-inductor.

be seen that the analysis of the self inductance of the coupled-inductor in section III B is verified.

V. CONCLUSIONS

In this paper, an improved passive snubber with a coupled-inductor is investigated based on a single-phase single-stage full-bridge boost PFC converter. The theoretical analysis and experimental results show that: 1) The adoption of this snubber can realize both the suppression of the voltage spike across the primary side of the power transformer and the energy transfer from the snubber itself to the load, and 2) The use of a coupled-inductor in the improved snubber to replace the two single-inductors can help achieve the synchronous resonances in the snubber. It can also help avoid the unbalance of the voltage and current among the devices of the snubber.

ACKNOWLEDGMENT

This work was supported by the National Natural Science Foundation of China (51107017) and China Postdoctoral Science Foundation Funded Project (2012M510954).

REFERENCES

[1] M. A. Al-Saffar, E. H. Ismail, and A. J. Sabzali, "Integrated buck-boost quadratic buck PFC rectifier for universal input applications," *IEEE Trans. Power Electron.*, Vol. 24, No. 12, pp. 2886-2896, Dec. 2009.

[2] B. H. Lee, C. E. Kim, K. B. Park, and G. W. Moon, "A new single-stage PFC AC/DC converter with low link-capacitor voltage," *Journal of Power Electronics*, Vol. 7, No. 4, pp. 328-335, Oct. 2007.

[3] D. Wijeratne, and G. Moschopoulos, "A three-phase single-stage AC-DC full bridge converter with high power factor and phase-shift PWM," in *Proc. IEEE APEC*, pp. 977-983, 2009.

[4] L. Z. Zhu, K. R. Wang, F. C. Lee, and J. S. Lai, "New

start-up schemes for isolated full-bridge boost converters," *IEEE Trans. Power Electron.*, Vol. 18, No. 4, pp. 946-951, Jul. 2003.
[5] T. Meng, H. Q. Ben, D. Q. Wang, and H. Huang, "Starting strategies of three-phase single-stage PFC converter based on isolated full-bridge boost topology," *Przeglad Elektrotechniczny (Poland)*, Vol. 87, No. 3, pp. 281-285, Mar. 2011.
[6] K. R. Wang, L. Z. Zhu, D. Y. Qu, H. Odendaal, J. Lai, and F. C. Lee, "Design, implementation, and experimental results of bi-directional full-bridge DC/DC converter with unified soft-switching scheme and soft-starting capability," in *Proc. IEEE PESC*, pp. 1058-1063, 2000.
[7] M. Nymand, and M. A. E. Andersen, "High-efficiency isolated boost DC-DC converter for high-power low-voltage fuel-cell applications," *IEEE Trans. Ind. Electron.*, Vol. 57, No. 2, pp. 505-514, Feb. 2010.
[8] V. Yakushev, V. Meleshin, and S. Fraidlin, "Full-bridge isolated current fed converter with active clamp," in *Proc. IEEE APEC*, pp. 560-566, 1999.
[9] E. S. Park, S. J. Choi, J. M. Lee, and B. H. Cho, "A soft-switching active-clamp scheme for isolated full-bridge boost converter," in *Proc. IEEE APEC*, pp. 1067-1070, 2004.
[10] D. Q. Wang, H. Q. Ben, and T. Meng, " A novel three-phase power factor correction converter based on active clamp technique," in *Proc. IEEE ICEMS*, pp. 1896-1901, 2008.
[11] A. Mousavi, P. Das, and G. Moschopoulos, "A comparative study of a new ZCS DC-DC full-bridge boost converter with a ZVS active-clamp converter," *IEEE Trans. Power Electron.*, Vol. 27, No. 3, pp. 1347-1358, Mar. 2012.
[12] A. Averberg, K. R. Meyer, and A. Mertens, "Current-fed full bridge converter for fuel cell systems," in *Proc. IEEE PESC*, pp. 866-872, 2008.
[13] M. Baei, and G. Moschopoulos, "A ZVS-PWM full-bridge boost converter for applications needing high step-up voltage ratio," in *Proc. IEEE APEC*, pp. 2213-2217, 2012.
[14] B. Su, and Z. Y. Lu, "An improved single-stage power factor correction converter based on current-fed full-bridge topology," in *Proc. IEEE PESC*, pp. 472-475, 2008.
[15] C. M. Qiao, and K. M. Smedley, "An isolated full bridge boost converter with active soft switching," in *Proc. IEEE PESC*, pp. 896-903, 2001.
[16] G. Moschopoulos, and P. Jain, "Single-stage ZVS PWM full-bridge converter," *IEEE Trans. Aero. Elec. Sys.*, Vol. 39, No. 4, pp. 1122-1133, Oct. 2003.
[17] R. Y. Chen, R. L. Lin, T. J. Liang, J. F. Chen, and K. C. Tseng, "Current-fed full-bridge boost converter with zero current switching for high voltage applications," in *Proc. IEEE IAS*, pp. 2000-2006, 2005.
[18] J. F. Chen, R. Y. Chen, and T. J. Liang, "Study and implementation of a single-stage current-fed boost PFC converter with ZCS for high voltage applications," *IEEE Trans. Power Electron.*, Vol. 23, No. 1, pp. 379-386, Jan. 2008.
[19] S. Jalbrzykowski, and T. Citko, "Current-fed resonant full-bridge boost DC/AC/DC converter," *IEEE Trans. Ind. Electron.*, Vol. 55, No. 3, pp. 1198-1205, Mar. 2008.
[20] L. Z. Zhu, "A novel soft-commutating isolated boost full-bridge ZVS-PWM DC-DC converter for bidirectional high power applications," *IEEE Trans. Power Electron.*, Vol. 21, No. 2, pp. 422-429, Mar. 2006.
[21] D. Q. Wang, H. Q. Ben, T. Meng, and Z. B. Lu, "Single-stage full-bridge PFC technique based on clamp circuit," *Electric Power Automation Equipment (China)*, Vol. 30, No. 5, pp. 53-56, May. 2010.
[22] T. Meng, H. Q. Ben, D. Q. Wang, and J. M. Zhang, "Research on a novel three-phase single-stage boost DCM PFC topology and the dead zone of its input current," in *Proc. IEEE APEC*, pp. 1862-1866, 2009.
[23] T. Meng, H. Q. Ben, D. Q. Wang, and J. F. Song, "Novel passive snubber suitable for three-phase single-stage PFC based on an Isolated full-bridge boost topology," *Journal of Power Electronics*, Vol. 11, No. 3, pp: 264-270, May 2011.

Tao Meng was born in Liaoning Province, China, in 1980. He received his B.S., M.S. and Ph.D. in Electrical Engineering from the Harbin Institute of Technology, Harbin, China, in 2003, 2005 and 2010, respectively. Since 2007, he has been an Engineer with the School of Electrical Engineering and Automation, Harbin Institute of Technology. His current research interests include power factor correction techniques, high frequency AC/DC and DC/DC conversion techniques, magnetic integration techniques and their applications.

Hongqi Ben was born in Heilongjiang Province, China, in 1965. He received his B.S. in Electrical Engineering from the Shenyang University of Technology, Shenyang, China, in 1988, his M.S. in Electrical Engineering from the Harbin Institute of Technology, Harbin, China, in 1991, and his Ph.D. in Mechatronics Engineering from the Harbin Institute of Technology, in 1999. Since 2004, he has been a Professor with the School of Electrical Engineering and Automation, Harbin Institute of Technology. His current research interests include high frequency power conversion techniques and power factor correction techniques.

Chunyan Li was born in Heilongjiang Province, China, in 1980. She received her B.S. in Automation from Heilongjiang University, Harbin, China, in 2003, and her M.S. and Ph.D. in Electrical Engineering from the Harbin Institute of Technology, Harbin, China, in 2005 and 2010, respectively. Since 2010, she has been a Lecturer with the School of Mechanical and Electrical Engineering, Heilongjiang University. Her current research interests include the design and control of permanent magnet motors.

Guo Wei was born in Liaoning Province, China, in 1966. He received his B.S. and M.S. in Electromagnetic Measurement and Instruments from the Harbin Institute of Technology, Harbin, China, in 1988 and 1991, respectively, and his Ph.D. in Scientific Research from Saga University, Saga, Japan, in 2003. Since 2008, he has been a Professor with the School of Electrical Engineering and Automation, Harbin Institute of Technology. His current research interests include modern sensor techniques, intelligent testing theory and its application, and weak signal detection and processing.